Journal of The Electrochemical Society, **155** (5) B504-B508 (2008)
0013-4651/2008/155(5)/B504/5/$23.00 © The Electrochemical Society

Nondestructive Reconstruction and Analysis of SOFC Anodes Using X-ray Computed Tomography at Sub-50 nm Resolution

John R. Izzo, Jr.,[a] Abhijit S. Joshi,[a] Kyle N. Grew,[a] Wilson K. S. Chiu,[a,*,z] Andrei Tkachuk,[b] Siew H. Wang,[b] and Wenbing Yun[b]

[a]*Department of Mechanical Engineering, University of Connecticut, Storrs, Connecticut 06269-3139, USA*
[b]*Xradia Incorporated, Concord, California 94520, USA*

A high-resolution, nondestructive X-ray computed tomography (XCT) technique is applied to image the three-dimensional (3D) microstructure of a solid oxide fuel cell (SOFC) composed of a solid yttria-stabilized zirconia (YSZ) electrolyte and a porous nickel YSZ (Ni–YSZ) anode. The X-ray microscope uses the 8 keV Cu Kα line from a laboratory X-ray source, with a reflective condenser optic lens providing a spatial resolution of 42.7 nm. The reconstructed volume data is visualized as 3D images and further postprocessed in binary-image format to obtain structural parameters. The porosity is calculated using a voxel counting method, and tortuosity is evaluated by solving the Laplace equation. A 3D representation of the microstructure is used to calculate true structural parameters and carry out a detailed study of the gas transport within an SOFC electrode at the pore scale. Simulation of multicomponent mass transport and electrochemical reactions in the anode microstructure using the XCT data as geometric input illustrate the impact of this technique on SOFC modeling.
 [DOI: 10.1149/1.2895067]

Manuscript submitted October 22, 2007; revised manuscript received February 12, 2008. Available electronically March 28, 2008.

X-rays have long been used for imaging purposes due to their ability to see past the surface and capture the internal information of a material. X-ray computed tomography (XCT) is a widely used technique in many fields where high computing power makes it possible to process large amounts of volume reconstruction data to be represented three-dimensionally. Three-dimensional (3D) volume data provides valuable insight to the material structural composition that cannot be accurately captured or approximated by two-dimensional (2D) images.

Soft X-rays, typically with a longer wavelength and lower energy, have been used for cellular and other biological imaging applications. A recent push in nanotechnology has raised interest in the microstructural properties of denser nanoporous materials for several applications, where techniques similar to biological imaging have been applied.[1,2] Currently there are two successful approaches to high-resolution full-field X-ray imaging, one that requires coherence illumination[3,4] and another that uses a high-resolution Fresnel lens (zone plate).[5-7] In recent years, both imaging techniques have demonstrated rapidly improving resolution. Coherence illumination has achieved 30 nm resolution[8] but requires a source with a high brilliance, such as a third- or fourth-generation synchrotron source. Using Fresnel lenses, Chao et al.[2] reported 15 nm resolution using soft X-rays to image biological samples. The Fresnel lens technique does not require a source with a high degree of coherence; in fact, even a laboratory X-ray source can be used to achieve 50 nm imaging resolution using hard X-rays through dense materials such as porous solid oxide fuel cell (SOFC) electrodes, as is shown in this article. Both techniques benefit from high brilliance of the synchrotron sources, which directly translates to imaging throughput required for in situ imaging of functional devices in their operation condition in the future.

SOFCs can benefit from XCT imaging, because better performance is expected for components with properly designed pore structure and electrochemically active sites. The ability to image these porous structures in 3D to study the size, distribution, and connectivity of the pores and channels is critical in enabling SOFC technology. In the past, other imaging techniques have been used to obtain 3D volume data of SOFC material structures.[9] One such technique used in Ref. 8 and 10 utilizes a scanning electron microscope (SEM) and focused ion beam (FIB). Thin layers of the material are removed with the FIB to collect a series of SEM images that are later processed by a reconstruction algorithm to represent the layers as 3D volume data. The FIB/SEM technique[10] represents a major advance in SOFC material characterization in that all three phases [pores, Ni, and yttria-stabilized zirconia (YSZ)] can be visualized, and the technique provides an accurate estimate of not only the porosity but the location of all individual phases and of the triple-phase boundary (TPB) length. The nondestructive XCT technique presented in this article makes it possible to image the 3D interior microstructure of the SOFC anode at a sub-pore resolution of 42.7 nm without physically removing material. Because the imaging occurs in a nondestructive manner, there is a considerably lower chance of damage or changes taking place in the microstructure.

Method of Approach

XCT.— The X-ray microscope used in this study is configured as a full-field transmission microscope, and the main components are schematically shown in Fig. 1. Full-field X-ray microscope operation principles are reminiscent of the visible-light transmission optical microscope, where the source of visible light is replaced by a bright X-ray generator and the glass focusing lenses are substituted by special X-ray optics (Fresnel zone plates) capable of focusing and magnifying the X-rays onto a high-resolution charge-coupled

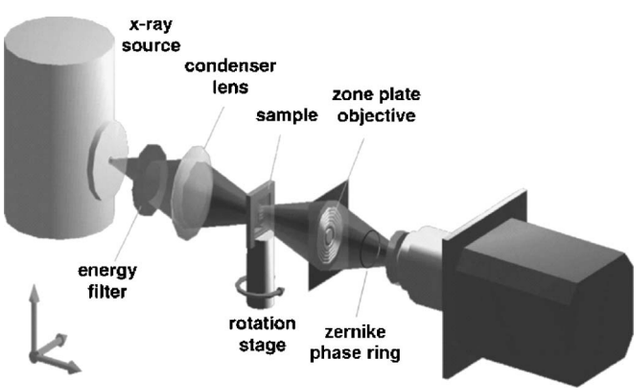

Figure 1. X-ray microscope experimental setup showing an 8 keV Cu Kα emission source with appropriate optics. The sample is mounted on a rotation stage where 181 2D projections are taken at 300 s exposure time per projection. The field of view is ~20 μm with 42.7 nm spatial resolution. A Zernike-phase ring is positioned in the back focal plane of the zone plate to enhance imaging contrast.

* Electrochemical Society Active Member.
z E-mail: wchiu@engr.uconn.edu

device (CCD) area detector. An X-ray copper rotating anode generator is used in conjunction with an energy filter that allows for the 8.05 keV (wavelength $\lambda = 1.54$ Å) Cu Kα emission line (see Ref. 6 for details). The X-rays enter a reflector condenser optic and are refocused onto the sample. The sample, mounted on a high-precision manipulator, is rotated through a range of angles. X-rays penetrate through the sample, and 2D projection images are magnified onto a high-resolution CCD detector using a Fresnel zone plate, acting as an objective lens. A gold phase plate with appropriate well-controlled thickness was positioned near the back focal plane of the zone plate to provide negative Zernike phase contrast enhancement.[1,5,6] This XCT system schieves Rayleigh criterion limited resolution of 42.7 nm.[11]

Imaging processing.— A reconstruction algorithm is used to create 3D volume data from the acquired projections based on X-ray density and image shadowing. A total of 181 2D projections at 300 s exposure time per projection were collected during sample rotation from $-90°$ to 90° and processed using a parallel beam filtered back-projection algorithm.[12,13] Hardware-accelerated tomography reconstruction software completes reconstruction time of a $512 \times 512 \times 512$ pixel volume on a modern 2.7 GHz single-processor PC in under 90 s. The sequence of slices and full reconstructed volume rotating in space is saved into binary data format for further data processing using ImageJ[c] and MATLAB.

A representative volume that consists entirely of the porous anode is chosen to perform the structural property calculations. This was because the porosity and tortuosity are properties of porous materials, Ni–YSZ anode in this study, and structural properties are greatly affected if nonporous regions like the solid YSZ electrolyte and empty space outside of the porous material are included in the volume used for analysis. A representative volume from the full data set is also required because of the computational cost in modeling applications using the XCT data as 3D geometry input.

The XCT volume data is first converted from gray-scale to binary voxels in order to calculate material properties like porosity and tortuosity, because it is required that the voxels represent either material or void space and nothing in between. The volume data in this form contains only two values, 1 or 0, representing the void (pore) space and the material, respectively. The conversion to binary requires the selection of a threshold value that accurately distinguishes between void space and material in the gray-scaled raw volume data set. Any value at or below the threshold is set to the void-space value, and any value above the threshold is set to the solid-material value, thus resulting in a binary volume of the actual porous microstructure to be further analyzed. The binary voxel data is used to generate a text file that contains the void space and material values for the actual SOFC anode microstructure and is used as the 3D geometry for gas transport or electrochemical modeling to predict the polarization curves for an SOFC with the microstructure obtained by XCT.

Structural parameter calculations.— The porosity (ϵ) is the ratio of the void volume to total volume. This microstructural parameter can be calculated by counting the number of solid and void voxels and dividing by the total number of voxels. Tortuosity (τ) is a measure of the path length of a pore to the material thickness, where a tortuosity value of one corresponds to a pore path length that is equal to the thickness. In this work, we use the Laplace equation to calculate tortuosity of the pore space, and because the calculation procedure is outlined in detail elsewhere,[14] it is not repeated here. The effective diffusivity D_{eff} of the porous medium can be calculated from the free diffusivity D (diffusivity in the absence of the porous medium) via the relation $D_{\text{eff}} = \Psi D$, where Ψ is the porosity–tortuosity factor ($\Psi = \varepsilon/\tau$). In the absence of the porous medium, $\Psi = 1$, and in general, Ψ is a function of the medium microstructure. Ψ depends on the direction, and a large variation with direction is to be expected for anisotropic materials.

Lattice Boltzmann method.— Multicomponent mass transport through the XCT reconstructed anode geometry is modeled using the lattice Boltzmann method (LBM). The LBM methodology[15] has been used to simulate SOFC mass transport in two dimensions[16] and has been recently extended to three dimensions.[14] LBM is selected over approaches such as Fick's law, the Stefan–Maxwell multicomponent diffusion model, or the dusty gas model because LBM can readily handle non-continuum multicomponent mass diffusion in complex 3D pore structures. The three species considered in the LBM model are H_2 (fuel), H_2O (product), and N_2 (inert gas). The fuel H_2 is fed to the gas side and diffuses from the gas side of the SOFC anode, through the pore structure, to the TPB. As a result of electrochemical reactions at the TPB, H_2 combines with oxygen ions to form H_2O. Electrons are released from the oxygen ion and flow through the Ni phase to the current collector. The H_2O diffuses back through the pores toward the gas side, where it is removed from the cell. It is assumed that diffusion occurs at a constant temperature and the mole flux of H_2 and H_2O is equal and opposite. The inert N_2 does not take part in electrochemical reactions at the TPB but influences transport of H_2 and H_2O through the pores. Because XCT provides a detailed representation of the geometric structure, mass transport through the porous anode is accurately modeled.

Electrochemistry model.— The multicomponent LBM model is also extended to incorporate detailed electrochemical reactions. Through the incorporation of a detailed electrochemical mechanism, the impact of the mechanism and the discrete placement of TPB locations can be examined. It is possible to consider more complex reaction mechanisms with multiple parallel spillover pathways;[17] however, significant questions about the detailed pathway still remain. Therefore, a mechanism developed through the examination and fitting of experimental electrochemical impedance spectroscopy data collected from pattern SOFC anodes is considered.[18,19] The detailed electrochemical reaction mechanism is coupled to the LBM model through the localized numeric evaluation of a set of four coupled differential equations that describe intermediate surface species concentrations using a pseudo steady-state approximation (PSSA). These coupled differential equations are dependent upon local gas-phase-species partial pressures through a surface reaction site density, kinetic-theory-based impingement rate, and coverage-dependent sticking probability.[20] The flux boundaries where this electrochemical reaction mechanism is coupled to the LBM are denoted through the domain by unique site identifiers in the LBM geometry files. Constant oxide ion and vacancy concentrations are assumed; however, the method is extendable to incorporate these effects. Using such a method, the impact of TPB site placement, TPB site density, and pore structure with respect to mass transfer, the activation process, and electrochemical reactions can be examined.

Results and Discussion

The sample imaged with the XCT system is the tip of a piece broken off from a hollow tubular SOFC, with a solid YSZ electrolyte shell and a thicker porous Ni–YSZ anode layer on the inside. The raw volume data is gray-scaled and composed of 492 2D slices that are 396×396 pixels, where the pixel size is 41.7 nm. The dimensions of the reconstructed cylindrical volume have a diameter of 15.6 μm and a length of 20.5 μm.

A movie of the rotating volume is constructed with a threshold value selected to distinguish between the material and void space, as shown with other movies of the SOFC sample.[d] The frame shown in Fig. 2a is taken from the movie generated from the raw volume data of the sample. The solid material is black and the void/empty space is white. SEM imaging performed on the sample confirms that the

[c] http://rsb.info.nih.gov/ij/.

[d] http://www.engr.uconn.edu/me/fuelcellimaging.php.

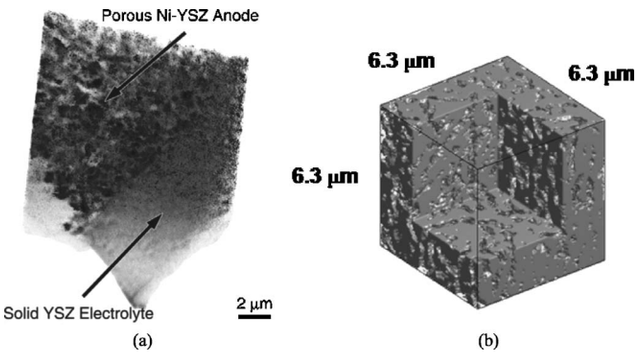

Figure 2. (a) A frame from the processed volume movie, where the material is black and void/empty space is white due to the selection of a threshold value that yielded a porosity matching experimental measurement for the sample, and (b) cut-away isosurface plot of the binary representative volume data.

outer shell is the solid YSZ electrolyte layer, while the inner layer is the porous Ni–YSZ anode. These solid and porous regions can be clearly identified and are labeled in Fig. 2a.

The volume data is further processed to study in detail the interior microstructure. A representative volume with the dimensions of 150 cubic pixels, corresponding to the cube with sides having a physical dimension of 6.3 μm, is selected from the raw volume data and converted to binary. The threshold value is selected to give the best representation of the microstructure by matching the bulk porosity of the binary volume to that measured for the sample calculated with mercury intrusion porosimetry (MIP) experiments.[21] The porous Ni–YSZ anode microstructure is much more defined in the binary format compared to the gray-scaled format of the volume data and is required for the geometry used in modeling mass transport through the pores. The anode microstructure is shown in Fig. 2b in the form of a cut-away isosurface plot of the representative binary volume to give a view of the interior microstructure. The cut-away image processing can remove any section of the volume and can be used to create orthogonal slices of any thickness of the binary volume data as well. The binary volume is processed to calculate the microstructural parameters critical to mass transport in the SOFC anode.

The porosity of the binary volume is calculated using a voxel counting method. Figure 3a shows the relationship between the calculated porosity and the size of the cube. Below a certain volume size the porosity of the sample fluctuates due to the local structure effects and is not representative of the entire SOFC anode. The porosity is required to be independent of the size of the volume to have a structure that is representative of the bulk SOFC anode. In order to determine this size, a study is performed by starting with the center voxel as the center of a cube and increasing the dimensions of the cube while measuring the porosity of each cubical volume. It was found that the porosity fluctuations stabilize when the side of the cube is 2 μm (approximately 50 voxels), resulting in a volume representative of the entire anode structure. As discussed earlier, this porosity value is also sensitive to the threshold selected when converting from grayscale to binary format. Because of this, some iteration is required in order to identify the right threshold value such that XCT calculations of porosity match experimental values. Based on the appropriate threshold value, the porosity of the XCT geometry is found to be about 30%.

Prediction of pore sizes using the XCT data is also validated to pore-size distributions obtained by MIP, as shown in Fig. 3b. The average pore size predicted by XCT and MIP is comparable. Calculations based on the XCT data show that the mean pore size is 0.34 μm. Note that large-diameter pores are not detected by MIP because this technique only detects the neck size of a converging or diverging pore, not a pore that undergoes convergence and then

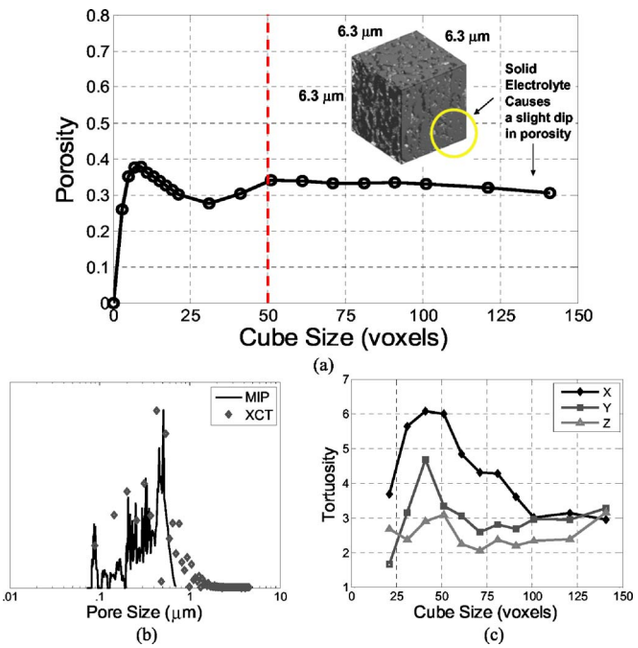

Figure 3. (Color online) (a) Fluctuations in the porosity of the representative volume calculated by increasing the size of the volume starting from the center voxel. A representative volume size of 50 voxels is adequate for accurately calculating the bulk porosity of the SOFC sample. One voxel represents a 41.7 nm × 41.7 nm × 41.7 nm cube. (b) Pore-size distribution inside a porous SOFC anode calculated using XCT and MIP. (c) Fluctuations in the tortuosity along *x*, *y*, and *z* of the representative volume calculated by increasing the size of the volume starting from the center voxel.

divergence; such pores are detected by XCT. In addition to calculating the pore-size distribution, the XCT data can be used to calculate the fraction of the pore volume that is topologically connected, forming a continuous pathway from one end of the sample to the other. This calculation reveals that 98% of the pore space is connected, 1.5% is composed of isolated pores (completely surrounded by solid phase), and 0.5% corresponds to dead-end pores; such information cannot be obtained by MIP. This information is useful for SOFC designs where connected pores should be maximized to enhance gas transport through the anode.

The XCT data is then used to estimate the tortuosity of the representative volume extracted from the sample. The tortuosity of the data (along *x*, *y*, and *z* directions) is estimated for different cube sizes, and the results are shown in Fig. 3c. Considerable differences are present in the tortuosity along different directions. In addition, unlike the porosity, the tortuosity values along *x*, *y*, and *z* do not attain a stable value, although the tortuosity values do converge to a common value with increasing sample size. This indicates that the sample size used for the tortuosity calculation is not large enough to be representative of the porous structure. When the entire sample is included, the tortuosity of the XCT data along the *x*, *y*, and *z* directions are 2.94, 3.28, and 3.15, respectively. The XCT-based estimate is much larger compared to $\tau = 1.77$ based on the pore-size distribution curve for the Ni–YSZ anode experimentally obtained using MIP. This discrepancy is thought to arise because the MIP pore-size distribution curve does not contain the larger pores between 0.7 and 2.0 micrometers as measured by XCT. When the larger pores are included in the calculation, we observed an increase in MIP-measured tortuosity to that obtained by XCT. The microstructural parameters, porosity and tortuosity, are commonly used to describe the mass transport in systems-level SOFC models. Clearly, the XCT data can provide an accurate means to calculate these values without recourse to empirical relationships, provided that a sufficiently large

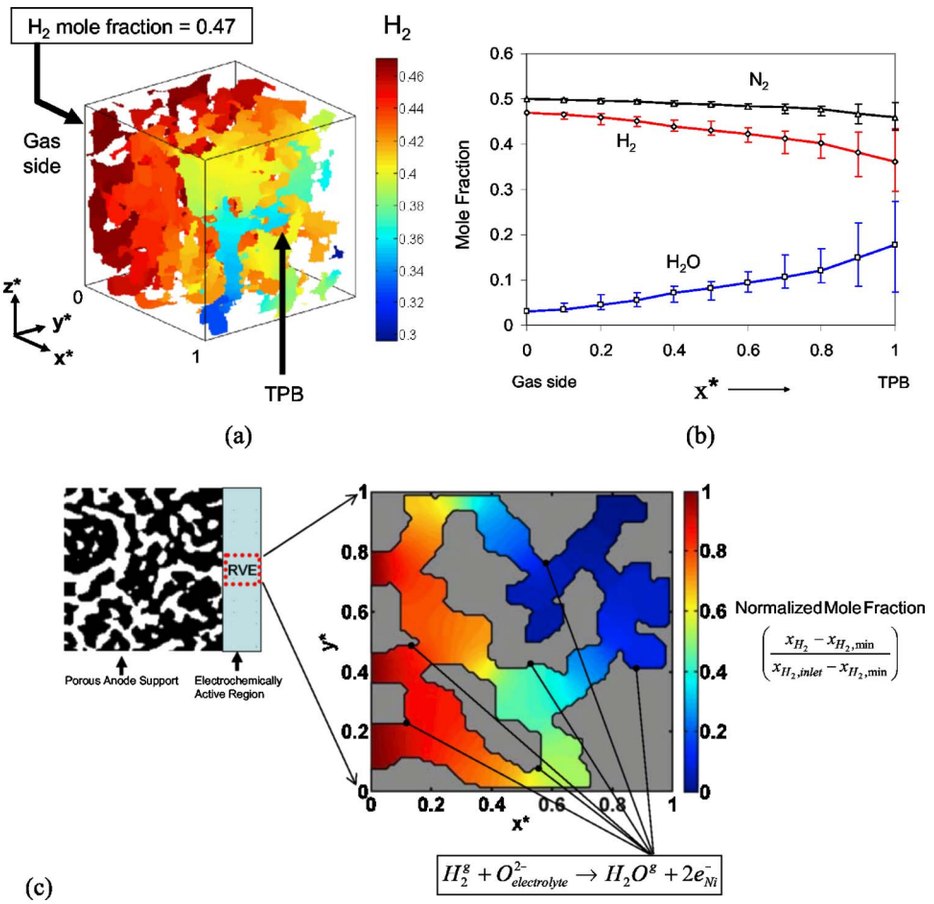

Figure 4. (Color online) Application of the XCT reconstructed geometry to predict (a) pore-scale species distribution of hydrogen in an SOFC anode using LBM.[13] (b) Average species mole fractions through the anode. (c) Application of 4×4 μm 2D subsection of XCT reconstruction to predict pore-scale species distributions of hydrogen and in the anode/electrolyte interface region using the coupled electrochemical model and LBM. Percolation pathways for electrons and ions are assumed in the out-of-plane dimension, and the entire interior region is assumed electrochemically active. (c) presents the variation of hydrogen concentration normalized to the maximum variation within the considered structure, where the specified H_2 mole fraction at the inlet is $x_{H_2,\text{inlet}} = 0.15$ and the minimum H_2 mole fraction within the pore domain is $x_{H_2,\text{min}} = 0.14869$.

volume of the porous material is imaged and reconstructed. Two examples of how the XCT data can be used as geometry input in SOFC analysis and design are presented next.

Based on the present XCT analysis, LBM is used to study mass transport through the porous SOFC anode.[14] A typical distribution of H_2 inside the porous anode obtained using LBM is shown in Fig. 4a. The length along the anode thickness is normalized using the anode thickness and is represented by x^*. The fuel species concentration of 47% H_2, 3% H_2O and 50% N_2 is known at $x^* = 0$ (gas side). The H_2 is consumed at the TPB to generate an equimolar amount of H_2O at the prescribed current density of the cell at $x^* = 1$. Figure 4b illustrates the species variation along the anode thickness x^*, along with lateral (y^*–z^*) variation of species as indicated by the uncertainty bars. Substantial lateral species variation can be seen especially near the TPB, indicating the importance of proper structural representation in analyzing gas transport in SOFCs. This information can be used to calculate the concentration polarization of the SOFC[14] through coupling of gas-transport models and electrochemistry. Because the current XCT technique only permits characterization of the pore and solid phases, only mass transport within the pore phase of the SOFC is studied. This permits calculation of the concentration polarization. As this XCT technique is developed further, geometric information about individual solid phases (Ni and YSZ) will be available, and the transport models can be further refined to predict charge transport through the electron and ion conducting phases and be able to calculate activation and ohmic polarization losses.

The capability of the coupled LBM and electrochemistry model is demonstrated with a 2D, 4×4 μm, section from the XCT microstructure data. The structure considered is assumed to be at the anode/electrolyte interface and have sufficient percolation pathways for the transport of electrons and ions to and from the current collector and electrolyte, respectively, in the out-of-plane direction. A homogeneous and even distribution of active sites is also assumed over the solid interface. Detailed phase-specific microstructures within the literature suggest such a distribution is a reasonable assumption.[22,23] Gas concentrations are prescribed at $x^* = 0$. A constant overpotential of 0.35 V is assumed for the charge-transfer mechanism, and a characteristic result is displayed in Fig. 4c where the normalized H_2 mole-fraction distribution is plotted. It can be noted in this figure how variations in the microstructure can lead to localized equilibration within subsections of the structure.

Conclusions

The microstructure of an SOFC sample with solid YSZ electrolyte and porous Ni–YSZ anode layers was imaged using a nondestructive X-ray tomography technique. This was performed with a laboratory XCT system using 8 keV X-rays produced from a rotating copper source, achieving a spatial resolution of 42.7 nm. The collected data was successfully postprocessed to enable visualization of the actual porous microstructure and analyzed in order to calculate structural parameters, then used as geometry input for predicting detailed, pore-scale mass transport and electrochemical reactions within the SOFC anode. The XCT reconstructed geometry can also be used to calculate the porosity and tortuosity of the porous SOFC electrodes for use as bulk parameters in simplified one-dimensional numerical models that calculate mass transfer through the pores. Structural parameters like porosity and pore-size distribution obtained using the XCT technique showed good agreement with prior results using MIP.

A detailed, nondestructive characterization of the porous SOFC electrode on the nanometer scale enables optimization of the electrode structure for achieving high power density and durability. Rec-

ommendations for future work include the nondestructive identification of the individual solid phases (Ni and YSZ) so that the TPB can be identified. This information will be valuable in pore-scale SOFC transport models, examples of which are presented in this work. With increasing availability of supercomputers and parallel computing platforms, detailed pore-level models will be at the forefront of SOFC analysis and optimization in the near future. The XCT technique developed in this work provides critical geometry input to such models.

Acknowledgments

Financial support from the Army Research Office is gratefully acknowledged. SOFC anode samples were provided by Adaptive Materials Inc. (Ann Arbor, MI). We thank Francesco De Carlo (Advanced Photon Source, Argonne, IL) for valuable discussions on image processing using ImageJ.

University of Connecticut assisted in meeting the publication costs of this article.

References

1. D. Rudolph, G. Schmahl, and B. Niemann, *Amplitude and Phase Contrast in X-Ray Microscopy*, pp. 59–67, Plenum, New York (1990).
2. W. Chao, B. D. Harteneck, J. A. Liddle, E. H. Anderson, and D. T. Attwood, *Nature (London)*, **435**, 1210 (2005).
3. D. Sayre and H. N. Chapman, *Acta Crystallogr.*, **A51**, 237 (1995).
4. J. Miao, K. O. Hodgson, T. Ishikawa, C. A. Larabell, M. A. LeGros, and Y. Nishino, *Proc. Natl. Acad. Sci. U.S.A.*, **100**, 110 (2003).
5. U. Neuhausler, G. Schneider, W. Ludwig, M. A. Meyer, E. Zschech, and D. Hambach, *J. Phys. D*, **36**, A79 (2003).
6. A. Tkachuk, M. Feser, H. Cui, F. Duewer, H. Chang, and W. Yun, *Proc. SPIE*, **6318**, 63181D (2006).
7. G.-C. Yin, M.-T. Tang, Y.-F. Song, F.-R. Chen, K. S. Liang, F. W. Duewer, W. Yun, C.-H. Ko, and H.-P. D. Shieh, *Appl. Phys. Lett.*, **88**, 241115 (2006).
8. R. K. Bansal, A. Kubis, R. Hull, and J. M. Fitz-Gerald, *J. Vac. Sci. Technol. B*, **24**, 554 (2006).
9. S. Griesser, G. Buchinger, T. Raab, and D. Meissner, *J. Fuel Cell Sci. Technol.*, **4**, 84 (2007).
10. J. R. Wilson, W. Kobsiriphat, R. Mendoza, H.-Y. Chen, J. M. Hiller, D. J. Miller, K. Thornton, P. W. Voorhees, S. B. Adler, and S. A. Barnett, *Nat. Mater.*, **5**, 541 (2006).
11. A. Tkachuk, F. Duewer, H. Cui, M. Feser, S. Wang, and W. Yun, *Z. Kristallogr.*, **222**, 650 (2007).
12. A. C. Kak and M. Slaney, *Principles of Computerized Tomographic Imaging*, IEEE Press, New York (1998).
13. M. Leeser, S. Coric, E. Miller, H. Yu, and M. Trepanier, *J. VLSI Signal Proc. Syst. Signal, Image, Video Technol.*, **39**, 295 (2005).
14. A. S. Joshi, K. N. Grew, J. R. Izzo, Jr., A. A. Peracchio, and W. K. S. Chiu, *J. Fuel Cell Sci. Technol.*, Submitted (2007).
15. A. S. Joshi, A. A. Peracchio, K. N. Grew, and W. K. S. Chiu, *J. Phys. D*, **40**, 2961 (2007).
16. A. S. Joshi, K. N. Grew, A. A. Peracchio, and W. K. S. Chiu, *J. Power Sources*, **164**, 631 (2007).
17. W. G. Bessler, J. Warnatz, and D. G. Goodwin, *Solid State Ionics*, **177**, 3371 (2007).
18. A. Bieberle and L. J. Gauckler, *Solid State Ionics*, **146**, 23 (2002).
19. W. G. Bessler, *Solid State Ionics*, **176**, 997 (2005).
20. K. N. Grew, A. S. Joshi, A. A. Peracchio, and W. K. S. Chiu, Paper IMECE2006-13621 presented at The ASME International Mechanical Engineering Congress and Exposition, Chicago, IL, Nov. 5–10, 2006.
21. J. R. Izzo, A. A. Peracchio, and W. K. S. Chiu, *Proceedings of the 42nd Power Sources Conference*, U.S. Army Research & Engineering Command, p. 139 (2006).
22. K. Reifsnider, X. Huang, G. Ju, and R. Solasi, *J. Mater. Sci.*, **41**, 6751 (2006).
23. M. Marinsek, S. Pejovnik, and J. Macek, *J. Eur. Ceram. Soc.*, **27**, 959 (2007).